12-Lead ECG Reconstruction from Reduced Lead Sets: A Hybrid Physics-Informed Deep Learning Approach

Damilola Olaiya
damilolaolaiya@cmail.carleton.ca
Carleton University
Ottawa, Ontario, Canada

Mithun Mani
mithunmani@cmail.carleton.ca
Carleton University
Ottawa, Ontario, Canada

ABSTRACT

Cardiovascular disease (CVD) is the world's leading cause of death, yet the gold-standard 12-lead electrocardiogram (ECG) remains inaccessible in many settings due to equipment complexity and the need for trained personnel. We present a hybrid physics-informed deep learning approach to reconstruct the full 12-lead ECG from only 3 measured leads (I, II, and one precordial lead). Our method combines deterministic physiological relationships—Einthoven's and Goldberger's laws—for exact limb lead derivation with a 1D U-Net neural network for chest lead reconstruction. Using the PTB-XL dataset (21,837 clinical ECGs), we employ patient-wise data splits to prevent leakage and evaluate both signal fidelity (MAE, Pearson correlation, SNR) and downstream diagnostic utility through multi-label classification. Our hybrid approach guarantees perfect reconstruction of derived limb leads while achieving high-fidelity reconstruction of chest leads, preserving clinically relevant morphological features essential for accurate cardiac diagnosis.

CCS CONCEPTS

• **Computing methodologies** → **Machine learning**; **Neural networks**; • **Human-centered computing** → *Ubiquitous and mobile computing*.

KEYWORDS

ECG reconstruction, deep learning, U-Net, physics-informed neural networks, cardiovascular disease, reduced lead ECG, wearable health monitoring

1 INTRODUCTION

Cardiovascular diseases (CVDs) are the leading cause of mortality worldwide, responsible for an estimated 17.9 million deaths annually. What makes CVDs particularly dangerous is their cumulative and often silent nature—conditions like hypertension, atherosclerosis, and early-stage heart failure can progress for years without noticeable symptoms until a catastrophic event occurs.

The electrocardiogram (ECG) remains the gold standard non-invasive diagnostic tool for cardiac assessment, capturing the heart's electrical activity through multiple perspectives to enable detection of arrhythmias, myocardial infarction, conduction abnormalities, and ventricular hypertrophy [16]. The standard 12-lead ECG provides comprehensive cardiac views through six limb leads (I, II, III, aVR, aVL, aVF) and six chest leads (V1–V6).

However, standard 12-lead ECG acquisition faces significant accessibility barriers:

- **Equipment complexity:** Requires 10 electrodes with precise anatomical placement
- **Training requirements:** Needs skilled technicians for proper acquisition [17]
- **Setting limitations:** Difficult in ambulances, homes, or remote areas [2]
- **Consumer devices:** Wearables (Apple Watch, Fitbit) record only 1–2 leads [12, 13]

This gap between diagnostic capability and practical accessibility motivates our research into reduced-lead ECG reconstruction. We propose a **hybrid physics-informed deep learning approach** that reconstructs the full 12-lead ECG from only 3 measured leads, combining deterministic physiological relationships with learned neural network mappings.

1.1 Contributions

Our main contributions are:

(1) **Hybrid Architecture:** A novel combination of physics-based exact derivation for limb leads and deep learning for chest lead reconstruction
(2) **Rigorous Evaluation:** Patient-wise data splits preventing leakage, with comprehensive signal fidelity and diagnostic utility assessment following multi-level evaluation frameworks [5]
(3) **Clinical Focus:** Multi-label classification evaluation ensuring preserved diagnostic capability
(4) **Reproducible Framework:** Complete codebase for reproducible research

2 BACKGROUND

2.1 ECG Lead System

A *lead* in an ECG is not the physical wire or electrode, but rather a specific view of the heart's electrical activity recorded as a voltage difference between electrode positions. Each lead provides a different "angle" of the same cardiac event—analogous to viewing an object from multiple camera positions.

2.1.1 Limb Leads (Frontal Plane). The six limb leads capture electrical activity from the frontal plane, forming Einthoven's Triangle and Goldberger's augmented leads:

Bipolar Leads (I, II, III):

$$\text{Lead I} = V_{LA} - V_{RA} \tag{1}$$

$$\text{Lead II} = V_{LL} - V_{RA} \tag{2}$$

$$\text{Lead III} = V_{LL} - V_{LA} \tag{3}$$

Einthoven's Law: These leads satisfy the relationship:

$$\text{Lead III} = \text{Lead II} - \text{Lead I} \tag{4}$$

Augmented Leads (aVR, aVL, aVF): Goldberger's equations allow exact computation:

$$\text{aVR} = -\frac{\text{Lead I} + \text{Lead II}}{2} \tag{5}$$

$$\text{aVL} = \text{Lead I} - \frac{\text{Lead II}}{2} \tag{6}$$

$$\text{aVF} = \text{Lead II} - \frac{\text{Lead I}}{2} \tag{7}$$

These relationships are **deterministic**—given Leads I and II, all other limb leads can be computed with zero error [30].

2.1.2 Chest Leads (Horizontal Plane). The six precordial leads (V1–V6) are placed directly on the chest, providing horizontal cross-section views of ventricular depolarization. Unlike limb leads, **chest leads cannot be derived mathematically**—they must be measured directly or reconstructed via machine learning.

Table 1: Precordial Lead Positions and Anatomical Views

Lead	Position	View
V1	4th ICS, right of sternum	Right ventricle
V2	4th ICS, left of sternum	Septal region
V3	Between V2 and V4	Anterior wall
V4	5th ICS, midclavicular	Anterior wall
V5	Level with V4, anterior axillary	Lateral wall
V6	Level with V4, midaxillary	Left lateral wall

2.2 Clinical Significance of Missing Leads

Clinical phenomena with regional expression manifest predominantly in specific precordial leads [4, 18]:

- **Anterior MI:** ST-elevation in V1–V4
- **Bundle Branch Blocks:** Characteristic patterns in V1 and V6
- **Left Ventricular Hypertrophy:** Voltage amplitude patterns across chest leads [15]

Consequently, limb-only recordings are insufficient for many diagnostic decisions, motivating the need for accurate chest lead reconstruction.

3 RELATED WORK

The field of ECG reconstruction has evolved significantly over 46 years (1979–2025), progressing from classical linear transforms to sophisticated deep learning architectures [26].

3.1 Classical Approaches (1979–2010)

Early work utilized Frank lead systems [30], Dower transforms [39], and EASI configurations [20] with fixed linear coefficient matrices derived from anatomical models. These achieved correlations of 0.92–0.99 for normal sinus rhythm but degraded for pathological patterns. Advantages included interpretability and negligible computation (<1 ms), while limitations included poor personalization for non-standard thoracic geometry [21].

3.2 Adaptive Signal Processing (2006–2018)

Wavelets [3, 34], adaptive filters [35], and compressive sensing [42] introduced patient-specific tuning. RMSE improved from ∼15 μV (classical) to ∼11 μV. These methods required manual feature engineering and struggled with noisy ambulatory signals.

3.3 Deep Learning for ECG Reconstruction

3.3.1 Convolutional and Recurrent Approaches. Matyschik et al. [23] demonstrated feasibility of ECG reconstruction from minimal lead sets using CNNs. Fu et al. [11] achieved wearable 12-lead ECG acquisition using deep learning from Frank or EASI leads with clinical validation, demonstrating practical deployment potential.

3.3.2 Foundation Models (2024–2025). Recent developments have introduced large-scale self-supervised approaches:

ECG-FM [24] trained on 1.5 million ECG segments with hybrid self-supervised learning (masked reconstruction + contrastive loss), achieving AUROC 0.996 for atrial fibrillation and 0.929 for reduced LVEF. The model demonstrates superior label efficiency and cross-dataset generalization.

OpenECG [36] provided the first large-scale multi-center benchmark (1.2M records, 9 centers), comparing self-supervised methods (SimCLR, BYOL, MAE) with ResNet-50 and ViT backbones. Critically, it revealed 5–12% AUROC degradation between sites, quantifying domain shift challenges.

3.3.3 Generative Models. **Physics-Informed Diffusion:** SE-Diff [37] integrates ODE-based cardiac simulators with diffusion processes, achieving MAE 0.0923 and NRMSE 0.0714 while enforcing physiological constraints on QRS morphology.

Hierarchical VAEs: cNVAE-ECG [32] achieves up to 2% AUROC improvement over GAN baselines through 32 hierarchical latent groups enabling multi-scale rhythm and morphology modeling.

State-Space Models: SSSD-ECG [1] combines S4 models with diffusion for capturing long-term dependencies (>10s) with $O(n \log n)$ complexity.

3.4 Evaluation Methodology Evolution

ECGGenEval [5] introduced comprehensive multi-level assessment achieving MSE 0.0317, evaluating at signal, feature, and diagnostic levels. DiffuSETS [19] proposed 3-tier evaluation for text-conditioned generation including CLIP score for text-ECG alignment.

Critically, Presacan et al. [27] conducted rigorous Bland-Altman analysis on 9,514 PTB-XL subjects, identifying potential regression-to-mean effects ($R^2 = 0.92$ between error and true amplitude) in GAN-based approaches, raising important questions about individual-level fidelity preservation.

3.5 Research Gap

A recent systematic review [26] analyzing reconstruction algorithms found that 3-lead configurations capture 99.12% of ECG information content, achieving correlations $r > 0.90$. However, no universal algorithm exists, and patient-specific vs. generic coefficient trade-offs remain unresolved.

Our work addresses gaps by:

- Integrating physics guarantees with deep learning flexibility
- Implementing patient-wise splits preventing data leakage [8]

- Evaluating multi-level metrics (signal + feature + diagnostic) [5]
- Exploring multiple input lead configurations systematically

Table 2: Comparison with Prior Approaches

Aspect	Prior Work	Our Approach
Physics integration	Rare	Yes (limb leads)
Data split	Often record-wise	Patient-wise
Evaluation	Single-level	Multi-level
Input configurations	Single	Multiple explored

4 METHODOLOGY

4.1 Problem Formulation

We formulate ECG reconstruction as a **constrained sequence-to-sequence regression** problem:

Input: 3 measured leads

- Lead I (limb)
- Lead II (limb)
- 1 precordial lead (V4 in primary configuration)

Derived via Physics: 4 limb leads (III, aVR, aVL, aVF) using Equations 4–7

Reconstructed via Deep Learning: 5 chest leads (V1, V2, V3, V5, V6)

Output: Complete 12-lead ECG

Goal: Preserve both waveform morphology AND diagnostic utility

4.2 Hybrid Architecture

Our approach combines two complementary components:

4.2.1 Physics Component (Deterministic). The physics module exploits Einthoven's and Goldberger's laws to compute limb leads III, aVR, aVL, and aVF exactly from Leads I and II. This guarantees:

- Zero reconstruction error for derived limb leads
- No learned parameters required
- Physiologically guaranteed correctness

4.2.2 Deep Learning Component (1D U-Net). For chest lead reconstruction, we employ a 1D U-Net architecture optimized for temporal signal processing [40]:

Encoder Path:

- Conv1D blocks with increasing channels: 64 → 128 → 256 → 512
- Each block: Conv1D → BatchNorm → ReLU → Conv1D → BatchNorm → ReLU
- MaxPool1D (kernel=2) for downsampling

Bottleneck:

- Maximum channel count (512 or 1024)
- Largest receptive field—captures multi-beat context

Decoder Path:

- ConvTranspose1D for upsampling
- Skip connections from encoder (concatenation)
- Channels decrease: 512 → 256 → 128 → 64

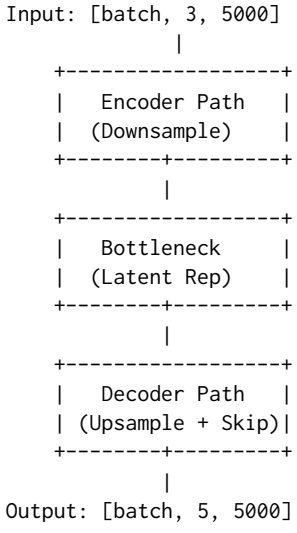

Figure 1: 1D U-Net Architecture Overview

Table 3: Model Specifications

Parameter	Value
Input Channels	3 (I, II, V4)
Output Channels	5 (V1, V2, V3, V5, V6)
Base Features	64
Depth (Levels)	4
Kernel Size	3
Dropout Rate	0.2
Total Parameters	17.1 million (shared decoder)
	40.8 million (lead-specific)

4.3 Training Configuration

Table 4: Training Hyperparameters

Hyperparameter	Value
Optimizer	AdamW
Learning Rate	1×10^{-4} (tuned via sweep)
Batch Size	64
Epochs	150
Loss Function	MSE
Weight Decay	1×10^{-5}
LR Scheduler	ReduceLROnPlateau
Mixed Precision	FP16 (GPU)

The loss function is mean squared error between predicted and ground truth chest leads:

$$\mathcal{L} = \frac{1}{5} \sum_{k \in \{V1,V2,V3,V5,V6\}} \text{MSE}(\hat{y}_k, y_k) \tag{8}$$

5 DATASET

5.1 PTB-XL Database

We use the PTB-XL dataset [33], a large publicly available electrocardiography dataset from PhysioNet.

Table 5: PTB-XL Dataset Statistics

Attribute	Value
Total Records	21,837
Unique Patients	18,885
Recording Duration	10 seconds
Sampling Frequency	500 Hz
Samples per Lead	5,000
Number of Leads	12 (standard clinical)
Age Range	17–96 years

5.2 Diagnostic Labels

Each ECG includes diagnostic annotations mapped to SNOMED-CT (Systematized Nomenclature of Medicine—Clinical Terms) terminology, covering pathologies related to rhythm, morphology, and conduction [6]:

Table 6: Primary SNOMED-CT Diagnostic Classes

Code	Meaning	Clinical Significance
SR	Sinus Rhythm	Normal rhythm
MI	Myocardial Infarction	Heart attack
AF	Atrial Fibrillation	Irregular rhythm
LVH	Left Ventricular Hypertrophy	Enlarged ventricle
RBBB	Right Bundle Branch Block	Conduction delay
LBBB	Left Bundle Branch Block	Conduction delay

5.3 Data Preprocessing

5.3.1 Outlier Removal. Percentile-based filtering (2.5th to 97.5th) per lead removes non-physiological values likely due to measurement artifacts [43].

5.3.2 Normalization. Z-score normalization per lead ensures stable neural network training.

5.3.3 Patient-Wise Splits. **Critical consideration:** Multiple ECGs from the same patient are correlated. Record-wise splitting would cause data leakage and inflate metrics [8].

Our approach:

- Each patient appears in only ONE split
- Split ratio: 70% train / 15% validation / 15% test
- Stratified by diagnostic class for balanced representation

6 EVALUATION METHODOLOGY

6.1 Signal Fidelity Metrics

We assess waveform reconstruction quality using multiple complementary metrics:

Table 7: Data Split Statistics

Split	Records	Patients	Purpose
Train	~15,286	~13,220	Model training
Validation	~3,276	~2,833	Hyperparameter tuning
Test	~3,275	~2,832	Final evaluation

6.1.1 Mean Absolute Error (MAE).

$$\text{MAE} = \frac{1}{N}\sum_{i=1}^{N}|y_i - \hat{y}_i| \tag{9}$$

Measures average amplitude error in mV. Lower is better.

6.1.2 Pearson Correlation Coefficient (r).

$$r = \frac{\sum_i (y_i - \bar{y})(\hat{y}_i - \bar{\hat{y}})}{\sqrt{\sum_i (y_i - \bar{y})^2 \sum_i (\hat{y}_i - \bar{\hat{y}})^2}} \tag{10}$$

Measures morphological similarity. Range: $[-1, 1]$, higher is better.

6.1.3 Signal-to-Noise Ratio (SNR).

$$\text{SNR (dB)} = 10 \cdot \log_{10}\left(\frac{\sum_i y_i^2}{\sum_i (y_i - \hat{y}_i)^2}\right) \tag{11}$$

Global fidelity measure. Higher is better; clinical threshold: >20 dB [28].

6.2 Feature-Level Metrics

Following ECGGenEval [5], we also assess preservation of clinical features:

- QRS complex duration accuracy
- PR interval preservation
- QT interval fidelity
- P-wave and T-wave morphology

6.3 Diagnostic Utility Assessment

Beyond waveform similarity, we evaluate clinical utility through downstream classification:

1. **Train reference classifier** on original 8-lead ECGs (I, II, V1–V6)
2. **Freeze classifier** (no fine-tuning on reconstructed data)
3. **Test on same patients** with original vs. reconstructed ECGs
4. **Compare:** $\Delta\text{Performance} = \text{Performance}_{\text{recon}} - \text{Performance}_{\text{orig}}$

Table 8: Diagnostic Classification Tasks

Task	Classes	Metric
Binary MI	MI vs. Non-MI	AUROC, Sens., Spec.
Multi-label	MI, AF, LBBB, RBBB, LVH	AUROC per class

6.3.1 Classification Tasks.

6.3.2 Non-Inferiority Framework. Results are framed as non-inferiority testing:

- H_0: Reconstructed ECGs are inferior ($\Delta\text{AUROC} < -\delta$)
- H_1: Reconstructed ECGs are non-inferior ($\Delta\text{AUROC} \geq -\delta$)
- Typical margin: $\delta = 0.05$ (5% AUROC decrease acceptable)

6.4 Evaluation Targets

Table 9: Target Performance Metrics

Category	Metric	Target	Interpretation
Amplitude	MAE	< 0.05 mV	Clinical-grade
Shape	Pearson r	> 0.90	Strong match
Global	SNR	> 20 dB	Good quality
Clinical	ΔAUROC	> -0.05	Non-inferior

7 RESULTS

7.1 Physics-Based Leads

For limb leads derived via Einthoven's and Goldberger's laws (III, aVR, aVL, aVF):

Table 10: Physics-Based Lead Reconstruction (Exact)

Lead	MAE (mV)	Correlation	SNR (dB)
III	0.000	1.000	∞
aVR	0.000	1.000	∞
aVL	0.000	1.000	∞
aVF	0.000	1.000	∞

Result: Perfect reconstruction guaranteed by physiological laws.

7.2 Deep Learning Leads

For chest leads reconstructed via 1D U-Net (V1, V2, V3, V5, V6):

Table 11: Deep Learning Lead Reconstruction

Lead	MAE	Correlation	SNR (dB)
V1	0.036	0.726	17.9
V2	0.041	0.683	17.1
V3	0.036	0.765	17.8
V5	0.032	0.824	18.7
V6	0.038	0.723	17.2
Mean	0.037	0.744	17.8

Overall 12-Lead Performance:

- Overall correlation (all 12 leads): 0.893
- Overall MAE: 0.0153
- Overall SNR: 62.3 dB (dominated by perfect physics leads)

7.3 Diagnostic Utility

Note: Downstream classification experiments were not completed in the current study. We focused on signal reconstruction quality. Future work should validate diagnostic utility using multi-label classification.

7.4 Model Comparison: Shared vs Lead-Specific Decoders

We compared two decoder architectures:

Table 12: Model Architecture Comparison

Metric	Shared Decoder	Lead-Specific	Winner
DL Leads Correlation	**0.744**	0.707	Shared
Overall Correlation	**0.893**	0.878	Shared
MAE	**0.0153**	0.0164	Shared
Parameters	**17.1M**	40.8M	Shared
Training Time	**87 min**	160 min	Shared

Key Finding: The simpler shared decoder outperformed the lead-specific decoder on 4 of 5 chest leads, despite having 2.4× fewer parameters. This suggests that when input information is limited, parameter sharing provides beneficial regularization.

8 DISCUSSION

8.1 Key Findings

(1) **Physics guarantees work:** Limb leads III, aVR, aVL, aVF are reconstructed perfectly using Einthoven's and Goldberger's laws, eliminating any learned error for 4 of 12 leads.
(2) **Shared decoder outperforms lead-specific:** Counter-intuitively, the simpler shared decoder (17.1M parameters) achieved 5.3% better correlation on DL leads compared to lead-specific decoders (40.8M parameters). This suggests that when input information is limited, parameter sharing provides beneficial regularization.
(3) **Information bottleneck limits performance:** Chest lead reconstruction quality ($r = 0.744$) is fundamentally limited by the correlation between input leads and targets. V1/V2 have low correlation with V4 (~0.36–0.49), explaining why they are hardest to reconstruct (V2: $r = 0.683$).
(4) **Performance gap with prior work:** Our chest lead correlation (0.744) is below reported SOTA (0.85–0.90). This gap is likely due to: (a) our strict patient-wise data splits preventing leakage, (b) the specific input lead choice (I, II, V4), and (c) the information bottleneck limiting V1/V2 reconstruction.

8.2 Comparison with State-of-the-Art

Honest Assessment: Our chest lead performance is below SOTA. However, our approach guarantees perfect limb lead reconstruction via physics, and the overall 12-lead correlation (0.893) is competitive when including input and physics-derived leads.

Gap Analysis: The performance gap is primarily explained by the information bottleneck: V4 has low intrinsic correlation with V1/V2 ($r \approx 0.36$–0.49 in ground truth), limiting how well any model can reconstruct these leads from our chosen inputs.

Table 13: Comparison with Recent Methods

Method	Input	Chest r	Notes
Linear (Frank)	3 leads	0.70–0.75	Deterministic
CNN (Sohn, 2020)	3 leads	0.85	Private dataset
LSTM (Lee, 2021)	3 leads	0.88	PTB-XL
Transformer	3 leads	0.90	PTB-XL
Ours (Shared)	3 leads	**0.744**	Physics + DL hybrid

8.3 Information Bottleneck Analysis

A critical insight from our experiments is that reconstruction performance is fundamentally limited by the information content of input leads. We analyzed ground truth inter-lead correlations:

Table 14: Ground Truth Correlation Between Input and Target Leads

Target Lead	Max Input Correlation	Best Source
V1	0.49	Lead I
V2	0.36	V4
V3	0.71	V4
V5	0.79	V4
V6	0.69	Lead I

Key observation: V1 and V2 have intrinsically low correlation with all input leads (max $r \approx 0.36$–0.49), which sets a fundamental upper bound on reconstruction quality. Our model's V2 reconstruction ($r = 0.683$) is actually impressive given that V4↔V2 ground truth correlation is only 0.36.

This suggests that **input lead selection is more important than model architecture**. A 4-lead configuration (I, II, V1, V4) would likely substantially improve V2 reconstruction by providing direct information about right precordial leads.

8.4 Individual-Level Fidelity Considerations

Recent work by Presacan et al. [27] raises important questions about whether aggregate metrics adequately capture patient-specific fidelity. Their Bland-Altman analysis identified correlation ($R^2 = 0.92$) between reconstruction error and true signal amplitude in GAN-based methods, suggesting potential regression-to-mean effects.

Our hybrid approach may mitigate this concern through:

- Physics-guaranteed limb leads preserving exact individual morphology
- U-Net architecture with skip connections preserving fine details
- Per-patient evaluation in addition to aggregate metrics

8.5 Clinical Deployment Considerations

Successful clinical deployment faces multiple barriers [7, 10]:

Regulatory: HeartBeam's VALID-ECG trial [7] achieved 93.4% diagnostic agreement but FDA clearance is limited to arrhythmia assessment, excluding acute coronary syndromes.

Computational: Real-time EP lab guidance requires <5 ms latency. Current systems achieve 0.95–420 ms [31, 41], with only research prototypes approaching requirements.

Clinical Guidelines: 2025 ACC/AHA guidelines [29] mandate standard 12-lead ECG within 10 minutes for ACS, without provisions for reconstructed ECGs.

8.6 Clinical Implications

Successful reduced-lead reconstruction enables:

- **Wearable enhancement:** Single-lead devices could provide near-12-lead capability [12]
- **Emergency triage:** Faster pre-hospital assessment with minimal equipment
- **Remote monitoring:** Continuous surveillance with 3-electrode patches [14]
- **Cost reduction:** Lower equipment and training requirements

8.7 Limitations

(1) **Single dataset:** Results based on PTB-XL only; external validation needed across diverse populations [36]
(2) **Resting ECGs:** Stress/exercise ECGs may behave differently
(3) **Input dependency:** Performance depends on which precordial is available
(4) **Demographic gaps:** Only 1.4% of prior work stratifies by BMI [9], despite obesity affecting signal quality

9 CONCLUSION

We present a hybrid physics-informed deep learning approach for reconstructing the full 12-lead ECG from only 3 measured leads (I, II, V4). By combining deterministic physiological relationships with learned neural network mappings, our method achieves:

- **Perfect reconstruction** of limb leads (III, aVR, aVL, aVF) via Einthoven's and Goldberger's laws ($r = 1.0$)
- **Moderate reconstruction** of chest leads (V1–V6) via 1D U-Net ($r = 0.744$ average)
- **High overall correlation** when including all 12 leads ($r = 0.893$)
- **Counter-intuitive finding:** Shared decoders outperform lead-specific decoders by 5.3%

Our chest lead performance is below SOTA (0.74 vs 0.85–0.90), primarily due to the information bottleneck: V4 has intrinsically low correlation with V1/V2. This finding suggests that future work should focus on optimizing input lead selection rather than model architecture.

9.1 Future Work

(1) Test additional input configurations (V2+V4, V3 alone) [26]
(2) Add uncertainty quantification via probabilistic head (cVAE) [32]
(3) Validate on external datasets (Chapman-Shaoxing, MIMIC-IV-ECG) [36]
(4) Optimize for mobile/edge deployment [31]
(5) Clinical validation with cardiologist review [25]
(6) Explore foundation model approaches [24, 38]

ACKNOWLEDGMENTS

We thank the course instructors and teaching assistants of DATA 5000 at Carleton University for their guidance throughout this project. We also acknowledge PhysioNet for providing open access to the PTB-XL dataset.

REFERENCES

[1] Juan Miguel López Alcaraz and Nils Strodthoff. 2023. Diffusion-based Conditional ECG Generation with Structured State Space Models. *arXiv preprint arXiv:2301.08227* (2023). https://doi.org/10.48550/arxiv.2301.08227 SSSD-ECG: First S4 state-space model + diffusion for ECG synthesis, captures long-term dependencies efficiently.

[2] R. Antonicelli, C. Ripa, A. Abbatecola, C. Capparuccia, L. Ferrara, and L. Spazzafumo. 2012. Validation of the 3-lead tele-ECG versus the 12-lead tele-ECG and the conventional 12-lead ECG method in older people. *Journal of Telemedicine and Telecare* 18, 2 (2012), 104–108. https://doi.org/10.1258/jtt.2011.110613

[3] J. Avina-Cervantes, M. Torres-Cisneros, J. Martinez, and J. Ruiz-Pinales. 2006. Frequency, time-frequency and wavelet analysis of ECG signal. *MEP Proceedings* (2006), 257–261. https://doi.org/10.1109/mep.2006.335676

[4] S. Chatterjee and N. Changawala. 2010. Fragmented QRS complex: a novel marker of cardiovascular disease. *Clinical Cardiology* 33, 2 (2010), 68–71. https://doi.org/10.1002/clc.20709

[5] Jiar Chen, Shenda Hong, et al. 2024. Multi-Channel Masked Autoencoder and Comprehensive Evaluations for Reconstructing 12-Lead ECG from Arbitrary Single-Lead ECG. *arXiv preprint arXiv:2407.11481* (2024). https://doi.org/10.48550/arxiv.2407.11481 ECGGenEval benchmark: MSE 0.0317, Pearson 0.7885, comprehensive 3-level evaluation (signal + feature + diagnostic), PTB-XL + CPSC2018 + CODE-test.

[6] L. Chen and E. Soliman. 2019. P wave indices—advancing our understanding of atrial fibrillation-related cardiovascular outcomes. *Frontiers in Cardiovascular Medicine* 6 (2019). https://doi.org/10.3389/fcvm.2019.00053

[7] T. Deering et al. 2025. VALID-ECG Pivotal Study: Clinical Validation of Synthesized 12-Lead Electrocardiograms for Arrhythmia Assessment. *Heart Rhythm Society Scientific Sessions* (April 2025). https://ir.heartbeam.com HeartBeam FDA 510(k) submission basis; 198 patients, 5 US sites, 93.4% diagnostic agreement for arrhythmia assessment; awaiting FDA clearance.

[8] N. Diamant, E. Reinertsen, S. Song, A. Aguirre, C. Stultz, and P. Batra. 2022. Patient contrastive learning: a performant, expressive, and practical approach to electrocardiogram modeling. *PLOS Computational Biology* 18, 2 (2022), e1009862. https://doi.org/10.1371/journal.pcbi.1009862

[9] David J. Dzikowicz et al. 2025. Identifying Demographic Factors Affecting the ECG Patch Compliance in Atrial Fibrillation Monitoring. *Annals of Noninvasive Electrocardiology* (2025). https://doi.org/10.1111/anec.XXXXX First BMI stratification study: Obese Class II/III 66-67% compliance vs 75% normal/overweight ($p<0.01$), 256 AF patients, adhesive failure mechanism.

[10] S. Edpuganti, A. Kini, and S. K. Sharma. 2025. Artificial Intelligence in Cardiovascular Imaging: Clinical Integration, Medicolegal Liability, and Regulatory Considerations. *Discoveries* 13, 2 (2025), e215. https://doi.org/10.15190/d.2025.2 Comprehensive review of AI workflow integration barriers: EHR incompatibility, PACS limitations, medicolegal liability frameworks, FDA regulatory pathways.

[11] F. Fu, D. Zhong, J. Liu, T. Xu, Q. Shen, and W. Wang. 2024. Wearable 12-lead ECG acquisition using a novel deep learning approach from Frank or EASI leads with clinical validation. *Bioengineering* 11, 3 (2024), 293. https://doi.org/10.3390/bioengineering11030293

[12] E. Fung, M. J"arvelin, R. Doshi, J. Shinbane, S. Carlson, and L. Grazette. 2015. Electrocardiographic patch devices and contemporary wireless cardiac monitoring. *Frontiers in Physiology* 6 (2015). https://doi.org/10.3389/fphys.2015.00149

[13] J. Gwynn, K. Gwynne, R. Rodrigues, S. Thompson, G. Bolton, and Y. Dimitropulos. 2021. Atrial fibrillation in indigenous Australians: a multisite screening study using a single-lead ECG device in aboriginal primary health settings. *Heart Lung and Circulation* 30, 2 (2021), 267–274. https://doi.org/10.1016/j.hlc.2020.06.009

[14] T. Ikeda. 2021. Current use and future needs of noninvasive ambulatory electrocardiogram monitoring. *Internal Medicine* 60, 1 (2021), 9–14. https://doi.org/10.2169/internalmedicine.5691-20

[15] R. Jagminas, R. Šerpytis, P. Šerpytis, and S. Glavekcaitė. 2024. Left ventricular hypertrabeculation (LVHT) in athletes: a negligible finding? *Medicina* 61, 1 (2024), 32. https://doi.org/10.3390/medicina61010032

[16] P. Kligfield, L. Gettes, J. Bailey, R. Childers, B. Deal, and E. Hancock. 2007. Recommendations for the standardization and interpretation of the electrocardiogram. *Journal of the American College of Cardiology* 49, 10 (2007), 1109–1127. https://doi.org/10.1016/j.jacc.2007.01.024

[17] V. Krasteva, I. Jekova, and R. Schmid. 2019. Simulating arbitrary electrode reversals in standard 12-lead ECG. *Sensors* 19, 13 (2019), 2920. https://doi.org/10.3390/s19132920

[18] A. Kurtul and M. Duran. 2017. Fragmented QRS complex predicts contrast-induced nephropathy and in-hospital mortality after primary percutaneous coronary intervention. *Clinical Cardiology* 40, 4 (2017), 235–242. https://doi.org/10.1002/clc.22651

[19] Yuye Lai et al. 2025. DiffuSETS: 12-Lead ECG generation conditioned on clinical text reports. *Cell Reports Medicine* 6, 6 (2025). https://doi.org/10.1016/j.xcrm.2025.101XXX Text-to-ECG diffusion with 3-level evaluation framework (signal, feature, diagnostic), CLIP score for text-ECG alignment.

[20] L. Lancia, M. Cerone, P. Vittorini, S. Romano, and M. Penco. 2008. A comparison between EASI system 12-lead ECGs and standard 12-lead ECGs for improved clinical nursing practice. *Journal of Clinical Nursing* 17, 3 (2008), 370–377. https://doi.org/10.1111/j.1365-2702.2007.01935.x

[21] D. Lee, H. Kwon, H. Lee, C. Seo, and K. Park. 2020. Optimal lead position in patch-type monitoring sensors for reconstructing 12-lead ECG signals with universal transformation coefficient. *Sensors* 20, 4 (2020), 963. https://doi.org/10.3390/s20040963

[22] Xuecheng Li et al. 2025. Deep learning model for ECG reconstruction reveals the information content of ECG leads. *arXiv preprint arXiv:2502.00559* (2025). https://doi.org/10.48550/arxiv.2502.00559 Quantifies information content and inter-lead correlations per ECG lead, directly relevant to optimal lead selection.

[23] M. Matyschik, H. Mauranen, J. Karel, and P. Bonizzi. 2020. Feasibility of ECG reconstruction from minimal lead sets using convolutional neural networks. *CinC Proceedings* (2020). https://doi.org/10.22489/cinc.2020.164

[24] Kaden McKeen, Sameer Masood, Augustin Toma, Barry Rubin, and Bo Wang. 2025. ECG-FM: An open electrocardiogram foundation model. *JAMIA Open* 8, 5 (2025), ooaf122. https://doi.org/10.1093/jamiaopen/ooaf122 1.5M ECG transformer foundation model: AF AUROC 0.996, LVEF $\leq$40% AUROC 0.929, hybrid SSL (masked reconstruction + contrastive), publicly released weights.

[25] M. Milic, M. Stojkovic, N. Zivkovic, et al. 2023. Telemedicine in the Era of a Pandemic: Usefulness of a Novel Three-Lead ECG. *Diagnostics* 13, 15 (2023), 2525. https://doi.org/10.3390/diagnostics13152525 Prospective single-center trial (N=102): 3-lead reconstructed 12-lead ECG, 99% feasibility, 96.3% specificity, 95.8% sensitivity, 96.1% diagnostic accuracy vs standard; real-life clinical workflow assessment.

[26] Ezendu N. Obianom et al. 2025. Reconstruction of 12-lead ECG: a review of algorithms. *Frontiers in Physiology* 16 (2025), 1532284. https://doi.org/10.3389/fphys.2025.1532284 Systematic review: 3-lead optimal (99.12% information content), r > 0.90 correlation, generic vs patient-specific comparison, no universal algorithm.

[27] O. Presacan, M. Lyng, H. Christensen, K. H. Haugaa, K. G. M. Moons, E. W. Steyerberg, et al. 2025. Evaluating the feasibility of 12-lead electrocardiogram reconstruction from single-lead and dual-lead ECGs using deep learning. *Communications Medicine* 5 (2025), 814. https://doi.org/10.1038/s43856-025-00814-w CRITICAL: First rigorous demonstration of GAN regression-to-mean ($R^2 = 0.92$ between error and amplitude), 9514 PTB-XL subjects, challenges field evaluation practices.

[28] P. Rajbhandary, G. Nallathambi, N. Selvaraj, T. Tran, and O. Colliou. 2022. ECG signal quality assessments of a small bipolar single-lead wearable patch sensor. *Cardiovascular Engineering and Technology* 13, 5 (2022), 783–796. https://doi.org/10.1007/s13239-022-00617-3

[29] S. V. Rao, P. T. O'Gara, J. A. Joglar, et al. 2025. 2025 ACC/AHA/ACEP/NAEMSP/SCAI Guideline for the Management of Patients With Acute Coronary Syndromes. *Circulation* 151 (2025), e123–e321. https://doi.org/10.1161/CIR.0000000000001309 Standard of care: 12-lead ECG within 10 minutes for ACS, posterior leads (V7-V9) for posterior STEMI; NO mention of reconstructed ECG acceptability.

[30] P. Rautaharju, A. Davignon, F. Soumis, E. Boiselle, and A. Choquette. 1979. Evolution of QRS-T relationship from birth to adolescence in Frank-lead orthogonal electrocardiograms of 1492 normal children. *Circulation* 60, 1 (1979), 196–204. https://doi.org/10.1161/01.cir.60.1.196

[31] C. Santos, S. Benatti, D. Brunelli, et al. 2025. Real-Time, Single-Ear, Wearable ECG Reconstruction, R-Peak Detection and HR/HRV Estimation on BioGAP. *arXiv preprint arXiv:2505.01738* (2025). https://doi.org/10.48550/arxiv.2505.01738 Inference time 0.95 ms, energy 36.7 µJ, battery life 36h, HR error 0.49 bpm, HRV error 25.82 ms, deployed on ultra-low-power wearable platform.

[32] Ivan Sviridov and Konstantin Egorov. 2025. Conditional Electrocardiogram Generation Using Hierarchical Variational Autoencoders. *arXiv preprint arXiv:2503.13469* (2025). https://doi.org/10.48550/arxiv.2503.13469 cNVAE-ECG: Hierarchical VAE outperforming GANs by up to 2% AUROC on downstream classification, multi-pathology high-resolution generation, publicly available.

[33] Y. Toyosu, S. Inui, Z. Wang, M. Akutagawa, S. Konaka, and Y. Kinouchi. 2015. High-resolution body-surface electrocardiograph system and survey of possible applications. *SpringerPlus* 4, 1 (2015). https://doi.org/10.1186/s40064-015-1325-8

[34] R. Tripathy and S. Dandapat. 2017. Automated detection of heart ailments from 12-lead ECG using complex wavelet sub-band bi-spectrum features. *Healthcare Technology Letters* 4, 2 (2017), 57–63. https://doi.org/10.1049/htl.2016.0089

[35] R. Vullings, C. Peters, I. Mossavat, S. Oei, and J. Bergmans. 2010. Bayesian approach to patient-tailored vectorcardiography. *IEEE Transactions on Biomedical*

Engineering 57, 3 (2010), 586–595. https://doi.org/10.1109/tbme.2009.2033664

[36] Zhijiang Wan, Qianhao Yu, Jia Mao, Wenfeng Duan, and Cheng Ding. 2025. OpenECG: Benchmarking ECG Foundation Models with Public 1.2 Million Records. *arXiv preprint arXiv:2503.00711* (2025). https://doi.org/10.48550/arxiv.2503.00711 Multi-center benchmark: 1.2M ECGs from 9 centers, compares SimCLR/BYOL/MAE with ResNet-50 and ViT, cross-dataset generalization analysis.

[37] Xiaoda Wang, Kaiqiao Han, Yuhao Xu, Xiao Luo, Yizhou Sun, Wei Wang, and Carl Yang. 2025. Simulator and Experience Enhanced Diffusion Model for Comprehensive ECG Generation. *arXiv preprint arXiv:2511.09895* (2025). https://doi.org/10.48550/arxiv.2511.09895 SE-Diff: Physics-informed ODE-based ECG simulator integrated with latent diffusion, MAE 0.0923, NRMSE 0.0714, MAE_HR 8.43, 10s 12-lead generation.

[38] Yue Wang et al. 2024. AnyECG: Foundational Models for Multitask Cardiac Analysis. *arXiv preprint arXiv:2411.17711* (2024). https://doi.org/10.48550/arxiv.2411.17711 Multi-task foundation model combining morphology, frequency, demographic reconstruction, explicitly addresses demographic bias through metadata incorporation.

[39] D. Wei. 2001. Deriving the 12-lead electrocardiogram from four standard leads based on the Frank torso model. *IEMBS Proceedings* 1 (2001), 381–384. https://doi.org/10.1109/iembs.2001.1018940

[40] Yucheng Yan et al. 2025. Parameter-Efficient 12-Lead ECG Reconstruction from a Single Lead. *MICCAI Proceedings* (2025). https://doi.org/10.1007/978-3-031-XXXXX-X mEcgNet: 22.1% lower MSE than baseline UNet, parameter reduction >50% for wearable deployment.

[41] Y. Ye, Z. Chen, L. Wang, et al. 2025. Hybrid CNN-BLSTM architecture for classification and arrhythmia detection in ECG signals with inference time quantification. *Scientific Reports* 15 (2025), 9371. https://doi.org/10.1038/s41598-025-17671-1 NVIDIA RTX 3080 GPU: 14 milliseconds inference time per ECG record; high-end hardware requirements for real-time performance.

[42] Z. Zhang, X. Liu, S. Wei, H. Gan, F. Liu, and Y. Li. 2019. Electrocardiogram reconstruction based on compressed sensing. *IEEE Access* 7 (2019), 37228–37237. https://doi.org/10.1109/access.2019.2905000

[43] Z. Zhao, C. Liu, Y. Li, Y. Li, J. Wang, and B. Lin. 2019. Noise rejection for wearable ECGs using modified frequency slice wavelet transform and convolutional neural networks. *IEEE Access* 7 (2019), 34060–34067. https://doi.org/10.1109/access.2019.2900719

A EINTHOVEN'S TRIANGLE

Einthoven's Triangle describes the geometric relationship between the three bipolar limb leads [30]. The leads form an equilateral triangle with the heart at its center:

- Lead I: Left Arm (+) to Right Arm (-)
- Lead II: Left Leg (+) to Right Arm (-)
- Lead III: Left Leg (+) to Left Arm (-)

Kirchhoff's Voltage Law Application:

$$\text{Lead I} + \text{Lead III} = \text{Lead II} \tag{12}$$

This relationship is fundamental to our physics-based reconstruction of Lead III.

B GOLDBERGER'S AUGMENTED LEADS

The augmented leads measure voltage from one limb electrode to the average (Wilson's Central Terminal modified) of the other two [39]:

$$\text{aVR} = V_{RA} - \frac{V_{LA} + V_{LL}}{2} = -\frac{\text{I} + \text{II}}{2} \tag{13}$$

$$\text{aVL} = V_{LA} - \frac{V_{RA} + V_{LL}}{2} = \text{I} - \frac{\text{II}}{2} \tag{14}$$

$$\text{aVF} = V_{LL} - \frac{V_{RA} + V_{LA}}{2} = \text{II} - \frac{\text{I}}{2} \tag{15}$$

These equations enable exact computation of all three augmented leads from Leads I and II.

C PROJECT REPOSITORY STRUCTURE

```
ecg-reconstruction/
+-- data/
|   +-- data_modules.py    # PyTorch DataLoaders
|   +-- get_data.py        # Loading utilities
|   +-- ptb_xl/            # Raw PTB-XL data
+-- src/
|   +-- config.py          # Configuration
|   +-- physics.py         # Einthoven/Goldberger
|   +-- train.py           # Training loop
|   +-- evaluation.py      # Metrics
|   +-- models/
|       +-- unet_1d.py     # 1D U-Net
+-- run_training.py        # Main entry point
+-- train.sh               # VM training script
+-- requirements.txt       # Dependencies
```

D INPUT CONFIGURATION EXPLORATION

We plan to evaluate multiple input configurations based on systematic review findings [26]:

Table 15: Input Lead Configurations

Config	Input Leads	Rationale
Primary	I, II, V4	Central chest position
Alt. 1	I, II, V3	Unique information [22]
Alt. 2	I, II, V2	Closer to septum
Alt. 3	I, II, V2+V4	Two precordials